

A Radial Time Projection Chamber for α detection in CLAS at JLab

R. Dupré,^{1,2} S. Stepanyan,³ M. Hattawy,^{1,2} N. Baltzell,^{1,3} S. Bueltmann,⁴ A. Celentano,⁵
 R. De Vita,⁵ H. Egiyan,³ H. Fenker,³ K. Hafidi,¹ S. Kuhn,⁴ Y. Perrin,⁶ B. Torayev,⁴ and E. Voutier^{2,6}
 (The CLAS Collaboration)

¹Argonne National Laboratory, Argonne IL 60439, USA

²Institut de Physique Nucléaire, CNRS/IN2P3 and Université Paris Sud, Orsay, France

³Jefferson Laboratory, Newport News, VA 230606, USA

⁴Old Dominion University, Norfolk, VA 23529, United States

⁵INFN, Sezione di Genova, 16146 Genova, Italy

⁶LPSC, Université Grenoble-Alpes, CNRS/IN2P3, Grenoble, France

(Dated: June 6, 2017)

A new Radial Time Projection Chamber (RTPC) was developed at Jefferson Laboratory to track low-energy nuclear recoils for the purpose of measuring exclusive nuclear channels, such as coherent Deeply Virtual Compton Scattering and coherent meson production on ${}^4\text{He}$. In such processes, the ${}^4\text{He}$ nucleus remains intact in the final state, however the CEBAF Large Acceptance Spectrometer (CLAS) cannot track the low energy α particles. In 2009, we carried out measurements using the CLAS spectrometer supplemented by the RTPC positioned directly around a gaseous ${}^4\text{He}$ target, allowing a detection threshold as low as 300 MeV/c for ${}^4\text{He}$. This article discusses the design, work principle, calibration methods and performances of this RTPC.

PACS numbers:

I. INTRODUCTION

Thomas Jefferson National Accelerator Facility (TJ-NAF), in Newport News, Virginia, USA, provides high power electron beams of energy up to 6 GeV and 100% duty cycle to three experimental Halls (A, B, C) simultaneously. The CLAS spectrometer [1], located in Hall-B, is composed of several sub-detectors and two magnets. Figure 1 shows a three dimensional representation of the baseline CLAS spectrometer:

- Three regions of Drift Chambers (DC) for the tracking of charged particles [2] (in blue on the figure).
- Superconducting toroidal magnet (in yellow) to bend the trajectories of charged particles, thus allowing momentum measurement with the DC tracking information.
- Cerenkov Counters (CC) to distinguish electrons from other negative particles, such as pions, at lower energies [3] (in pink).
- Scintillation Counters (SC) to identify hadrons by measuring their time of flight (TOF) [4] (in red).
- Electromagnetic Calorimeters (EC) to distinguish electrons from other negative particles at higher energies and to detect neutral particles (neutrons and photons in particular) [5] (in green).

Measurement of the Deeply Virtual Compton Scattering (DVCS) process ($eH \rightarrow e'H'\gamma$, where H is a hadron)

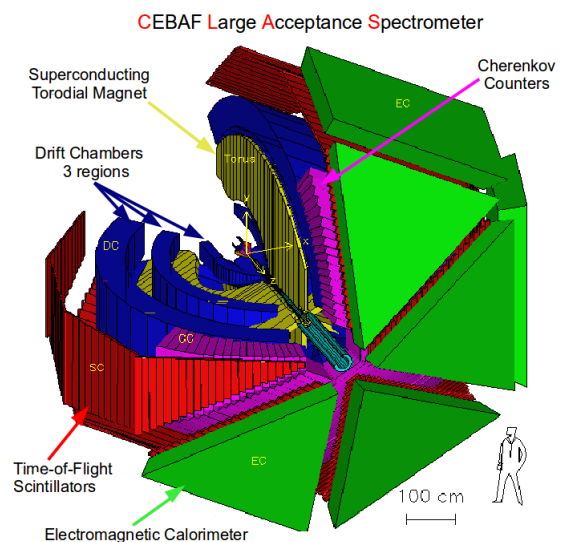


FIG. 1: A three dimensional representation of the baseline CLAS setup. The full description is given in the text.

necessitates an upgrade of this setup. With a 6 GeV electron beam, the majority of DVCS photons are produced at very forward angles, where the acceptance of the EC is poor. To extend the detection range, an inner calorimeter (IC) was built for the E01-113 experiment in 2005. The IC is constructed from 424 lead-tungstate (PbWO_4) crystals, covering polar angles between 5° and 15° . Each crystal is 16 cm long, corresponding to 17 radiation lengths. The achieved energy resolution is around 3 to 4% for photon energies between 2 GeV and 5 GeV,

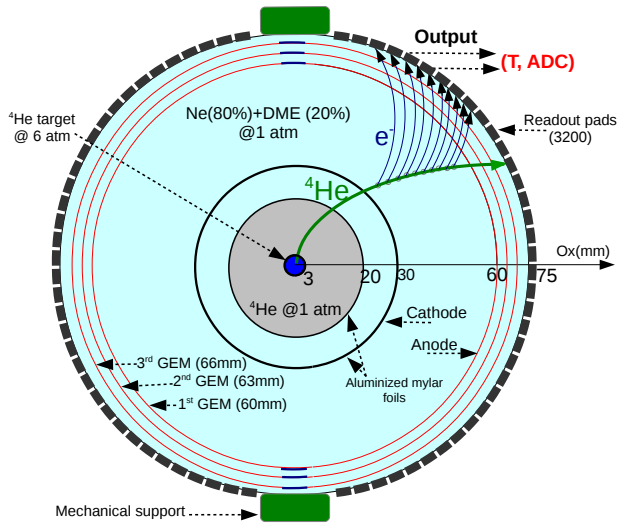


FIG. 2: Schematic drawing of CLAS RTPC in a plane perpendicular to the beam direction. See text for description of the elements.

with an angular resolution between 3 and 5 mrad [6]. To protect this detector from the large flux of low energy Møller electrons, a 5 T solenoid was placed around the target to shield the IC. In addition, the recoil nuclei of the coherent DVCS on helium was detected using a RTPC developed to track low energy nuclear fragments. The solenoid field serving as the analyzing magnet for the particle tracking in the RTPC. This setup was used during a three months experimental run [7, 8] in 2009 with a longitudinally polarized electron beam of 130 nA and energy of 6.064 GeV incident on a gaseous ^4He target.

In this paper we report the design, calibration, and performance of the radial TPC, organized as follows. In section II, we detail the design and internal structure of the detector. Section III describes the properties of the read-out system. Calibration strategies are discussed in section IV. Finally, the performances of the RTPC are described in section VI.

II. CLAS RTPC DESIGN

With a 6 GeV incident electron energy, the recoiling ^4He nuclei from coherent DVCS have an average momentum around 250 MeV/c. Such low energy α particles are stopped very rapidly, so the RTPC was designed to be as close as possible to the target and fitting within the 230 mm diameter of the 5 Tesla solenoid magnet surrounding the target.

The CLAS RTPC is a 250 mm long cylinder of 158 mm diameter, leaving just enough room to fit pre-amplifiers between the RTPC outer shell and the solenoid. The electromagnetic field is directed perpendicularly to the beam direction, such that drifting electrons are pushed away from the beam line. These electrons are ampli-

fied by three layers of curved GEMs and detected by the readout system on the external shell of the detector as illustrated in the figure 2. The CLAS RTPC is segmented into two halves with independent GEM amplification systems that cover about 80% of the azimuthal angle.

We detail here the different regions shown in figure 2 starting from the beam line and towards larger radius:

- First, the 6 atm helium-4 target extends along the beam line axis, it is 284 mm long with a 3 mm radius wall made of a $27\text{-}\mu\text{m}$ -thick Kapton.
- The first gas gap covers a radial range from 3 mm to 20 mm. It is filled with ^4He gas at 1 atm to minimize secondary interactions from Møller electrons scattered by the beam. This region is surrounded by a $4\text{ }\mu\text{m}$ thick window made of aluminized Mylar is electronically grounded.
- The second gap region extends between 20 mm and 30 mm and is filled with a gas mixture of 80% neon and 20% dimethyl ether (DME). This region is surrounded by a $4\text{ }\mu\text{m}$ thick window made of aluminized Mylar, which serves as the cathode and is set at 4260 V.
- The drift region is filled with the same Ne-DME gas mixture and extends from the cathode to the first GEM, 60 mm away from the beam axis. The average electric field in this region is about 550 V/cm and perpendicular to the beam.
- The electron amplification system is composed of three GEMs located at radii of 60, 63 and 66 mm. In this configuration, the first GEM layer serves as the anode and each subsequent GEM is set at a lower voltage to obtain a strong ($\sim 1600\text{ V/cm}$) electric field between the GEM foils. A 275 V bias is applied to each GEM for amplification.
- The readout board has an internal radius of 69 mm and collects charge from the GEMs. Pre-amplifiers are plugged directly on its outer side and transmit the signal to the data acquisition electronics.

The GEM technology has been chosen for its flexibility as it allows for a curved amplification surface. Also, GEMs are known to rarely create sparks [10], which is important when trying to detect highly ionizing slow nuclei that deposit large amount of energy. The GEMs for this RTPC are made from a Kapton insulator layer, $50\text{ }\mu\text{m}$ thick, sandwiched between two $5\text{ }\mu\text{m}$ copper layers. The mesh of each GEM layer is chemically etched with $50\text{ }\mu\text{m}$ diameter holes with double-conical shapes as illustrated in figure 3. The potential difference applied between the two copper layers of the GEM creates a very strong electric field in each hole leading to high ionization and amplification.

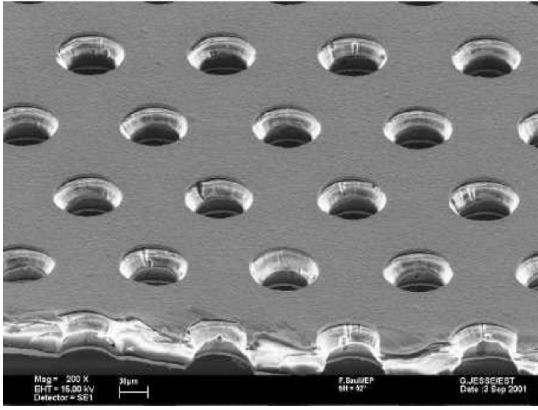


FIG. 3: Image of a typical GEM foil similar to the one used for our RTPC [9].

The drift gas used in the experiment is a 80-20% neon-DME mixture, this choice has been made in order to balance the energy deposit with a reasonable Lorentz angle. Calculations using the MAGBOLTZ program [11] showed that with the perpendicular 5 T field, we would have a Lorentz angle of about 23° with this gas mixture. This is already a significant angle, a heavier gas would have larger angle increasing significantly the length of the drift paths as the electron would make a long spiral around the beam line before to reach the GEMs.

One of the important problematic to develop the radial TPC was to obtain a good support structure of the GEM foils, allowing an easy installation of the GEM in good conditions and with high precision. At the same time, we wanted to keep the material budget small in the forward region where we detect other particles in subsequent detectors. We successfully realized these prerequisites by using fiber glass rings glued to each ends of the GEM foils to form self supporting cylinders that could be installed independently in the RTPC after all gluing and soldering operations. The rigidity of the GEM foil is enough for the structure to be self-supporting and only the backward part of the cylinder was fixed to the main mechanical structure. This design only left a light fiber-glass ring in the forward region, reducing to a minimum secondary interactions.

III. READOUT SYSTEM

The RTPC electron collection system has 3200 readout pads. These elements are located at the end of the amplification region, 69 mm from the central axis. Figure 4 shows a schematic drawing of the size and configuration of the pads. Each readout pad is 5 mm in length and 4.45 mm in width. The shift between the rows allows to reduce aliasing. Each half of the RTPC has 40 rows and 40 columns of pads. The shaded region in figure 4 shows how pads are grouped to 16 channels pre-amplifiers. The pre-amplifier boards, already employed in the BoNuS RTPC

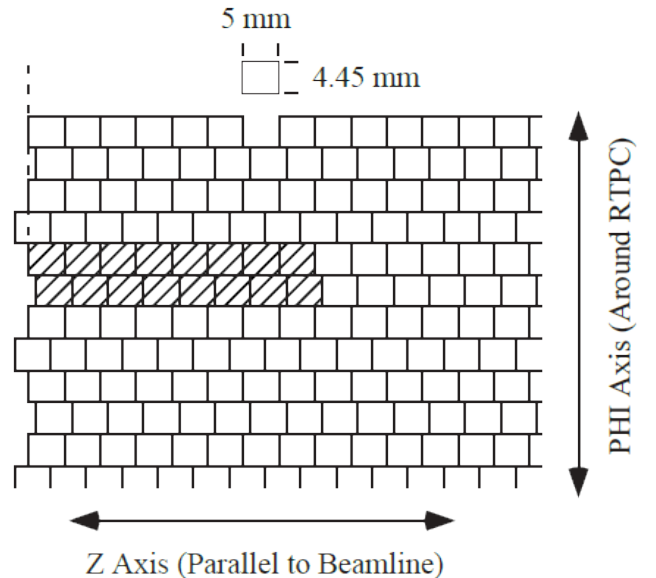


FIG. 4: A schematic representation of a part of the readout system. The shaded sixteen pads are a group of pads that are connected to the same pre-amplifier.

[12], serve the dual purpose of inverting the RTPC signals polarity – from negative to positive – to match the requirements of the subsequent readout system, and driving the 6 m long ribbon cable that connects to it.

The readout system is based on the Front End Electronic (FEE) boards originally developed for the ALICE TPC readout system at CERN [13]. Each readout channel is made of three main components: a charge sensitive, low impedance shaping amplifier, a 10 bit, 25-MHz digitizer, and a digital circuit that implements online-processing algorithms (pedestal subtraction, zero suppression, ad tail cancellation). The amplifier is implemented in a fully-analogue ASIC, PASA [14], while the subsequent signal digitization and elaboration part is implemented in a digital ASIC, ALTRO [15]. Both ASICs host 16 channels. The full readout chain is implemented on a single Front End Card (FEC), hosting 128 channels. FECs are hosted in custom crates, mounted close to the detector. A Readout Control Unit (ROC) board is used to distribute the trigger signal to FECs and for data readout. Each RCU can handle up to 25 FECs. Communication between ROC and FECs is performed trough a custom back-plane, implementing a low-voltage signal bus. The RCU communicates with the CLAS DAQ system trough a 200 MB/s optical link, connected to a data acquisition PC hosting a ReadOut Receiver Card (RORC). This PC hosts the readout controller application (ROC) used to interface with the CLAS DAQ system. An Ethernet link is also present, for slow-controls and monitoring.

Triggering and data-readout scheme is as follows. When a Level-1 (L1) trigger is received by a FEC-board, a programmable number of samples N_0 is digitized and

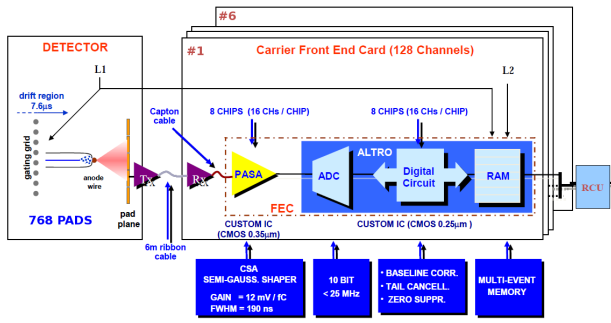


FIG. 5: Schematic representation of the RTPC readout system, showing

stored in a data memory, and hence processed by the digital circuit. Upon arrival of Level-2 trigger, the latest processed samples are saved in a multi-event memory, individual to each-channel, ready for readout by the RCU. In our setup, the RCU receives the trigger signal from the CLAS Trigger Supervisor system, and distributes both L1 and L2 signals to all the FECs in the crate, with a definite L1-L2 trigger latency. Such latency is programmable, and has to be long enough to accommodate the digitization of the N_0 samples per channel. In the current implementation, $N_0 = 100$ samples/channel are acquired for each trigger, operating ALTRO at the reduced sampling frequency of 10MHz . The L1-L2 latency is thus fixed to $15\ \mu\text{s}$.

The trigger signal also initiates RCU readout operation from FEC boards. All the measured samples from active channels are reported, together with a channel identifier and a time-stamp, to the ROC application, that in turns sends them on the main event builder. During data reconstruction, the acquired samples are processed to obtain, for each readout pad, the accumulated charge (ADC) and the pulse time (T). Since pulse time was obtained as the time-stamp of the first sample above threshold, the resolution is equivalent to the ALTRO sampling time, $100\ \text{ns}$.

In order to reduce the data size, ALTRO is operated in zero-suppression mode: only samples above a programmable threshold are stored in the ALTRO on-board memory and then written to tape. A glitch-filter permits to reject spurious pulses due to noise, by requiring the presence of a minimum number of samples over threshold N_{MINSEQ} to validate a sample. To properly reconstruct the signal shape, N_{PRE} samples before threshold-crossing and N_{POST} samples after the signal returns below threshold are saved. In the present configuration, $N_{MINSEQ} = N_{PRE} = N_{POST} = 3$, while threshold is set just above the noise level.

In order to read all the detector readout pads, four FEC crates are used, each equipped with 6 boards, plus a ROC. A schematic of the readout system, for a single crate, is reported in figure 5. This configuration permits to reduce the dead time associated to FEC readout operations, scaling linearly with the number of boards in the

crate. During the 2009 run, the system was successfully operated with a DAQ rate of $3.1\ \text{kHz}$, with a live time of 70%.

IV. CALIBRATION

The timing information is used to infer the origin of the charge and then the trajectory of the detected particle resulting in momentum measurement. Going from a collection of times to a momentum measurement requires a good knowledge of the drift speed and drift paths followed by the electrons released in the gas. The recorded ADCs give the deposited energy per unit of length ($\frac{dE}{dX}$) which, together with the momentum calculated from the trajectory, enables particle identification.

In this section we will detail the methods used to calibrate the drift speed, drift paths and gains of the detector. Drift speed and paths were initially calculated using the MAGBOLTZ [11] program, then refined using data to account for variations of the run conditions. We always assume cylindrical symmetry in the chamber for the calibration, such that none of the parameters depend on the azimuthal angle ϕ . The initial MAGBOLTZ calibration was improved through several iterations of the process described below, each iteration increasing the number of events properly reconstructed in the RTPC. The figures presented in this section are the one obtained while performing the last iteration of this long calibration process.

A. Drift Speed Parametrization

We determine the drift speed using tracks reconstructed in the RTPC. In figure 6, a typical ^4He track is represented (in green). After it causes ionization in the drift region, the released electrons (in black) drift to the cylindrical detection plane under the effect of the electric field. The electrons released close to the cathode take the most time to reach the readout pads, but cylindrical symmetry insures they always travel the same distance. By identifying the maximum time measured (T_{Max}), we can infer the drift speed of the electrons in the RTPC.

To measure the drift speed, we use the time profile of all hits in the chamber shown in figure 7. We can clearly observe the dropping edge expected from geometrical considerations. We define a value $T_{Max/2}$ at which the dropping edge passes half the maximum number of hits in the histogram. This value is measure in bins along the 200 mm RTPC's length to take into account variations in the electric and magnetic field in the RTPC (see figure 8).

Due to the non perfect experimental conditions, in particular variations in the gas mixture [17], the drift speed changes during the three months long experimental run. Figure 9 shows the $T_{Max/2}$ values for individual runs (approximately 2 hours long). We observe a significant vari-

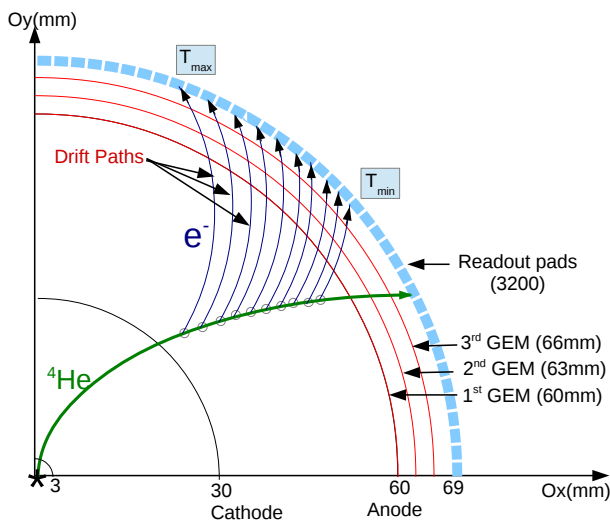


FIG. 6: A schematic drawing of a ^4He track (in green) traversing the drift region, with the drift paths followed by the electrons (in black).

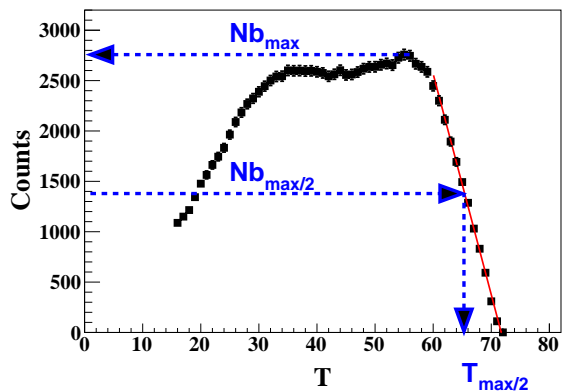


FIG. 7: Time profile of the collected hits in one experimental run.

ation of the drift speed over time and accounted for it in the drift speed used for the track reconstruction.

In summary, we obtain from our calibration a parametrization of the drift speed as a function of both position along the beam axis and run number (we did not observe any correlation between the effects). These functions were extracted for our entire data set and implemented in the track reconstructions code.

B. Drift Paths Calibration

The drift path is the trajectory followed by the electrons released through ionization in the gas. Software exists to calculate the drift paths, in particular MAGBOLTZ [11], but it requires knowledge of the detector's geometry, gas mixture composition, and of course the electric and magnetic fields over the whole volume of the

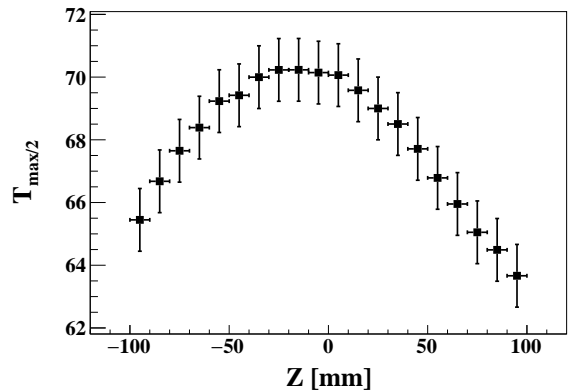


FIG. 8: Time profile distribution for the collected hits in one experimental run.

detector. We used such calculation as a first calibration, but, as can be seen with the drift speed, gas composition is far from stable in the chamber. Moreover, the $4\ \mu\text{m}$ foil used as a cathode is easily deformed, such that we expect the geometry accuracy to be of few millimeters, directly impacting our knowledge of the electric field. These problems, already encountered for the BoNuS RTPC calibration [12], motivated the acquisition of specific calibration runs. These were taken with a lower energy electron beam (1.20 and 1.27 GeV) to enhance the cross section of the elastic scattering ($e^4\text{He} \rightarrow e^4\text{He}$). In this process, the measurement of the electron kinematic allows to calculate the Helium nucleus kinematic. It is by comparing this calculated kinematic to the measured one that we fine tune the drift paths independently of our knowledge of the exact conditions in the chamber.

The drift paths are adjusted using a set of identified elastic events from our lower beam energy run. Based on the kinematic of the electrons in these events, we generate the helium nucleus in a GEANT4 simulation [16] of our RTPC. Then we compare the calculated GEANT4 trajectory of the Helium nuclei to the hits measured in the chamber.

Because of the magnetic field, the drift paths are not linear in the RTPC. So to perform the extraction, we make a first approximation with a linear dependence between the radius of emission and the time of detection, and then refine our result. As it happens, the curvature is minimal and this process converge already on the second iteration.

At the end of the extraction procedure, the azimuthal difference between the detection pad and the ionization point ($\Delta\phi$) is extracted as a function of time. In figure 10, we show the resulting data points for one bin, where the drift paths is easily identified and eventually fitted for implementation in our reconstruction codes.

To verify the stability of the drift paths, this procedure was carried out using both the 1.204 GeV data from the beginning of the run period and the 1.269 GeV data from the end of the run period (shown in blue on figure 9).

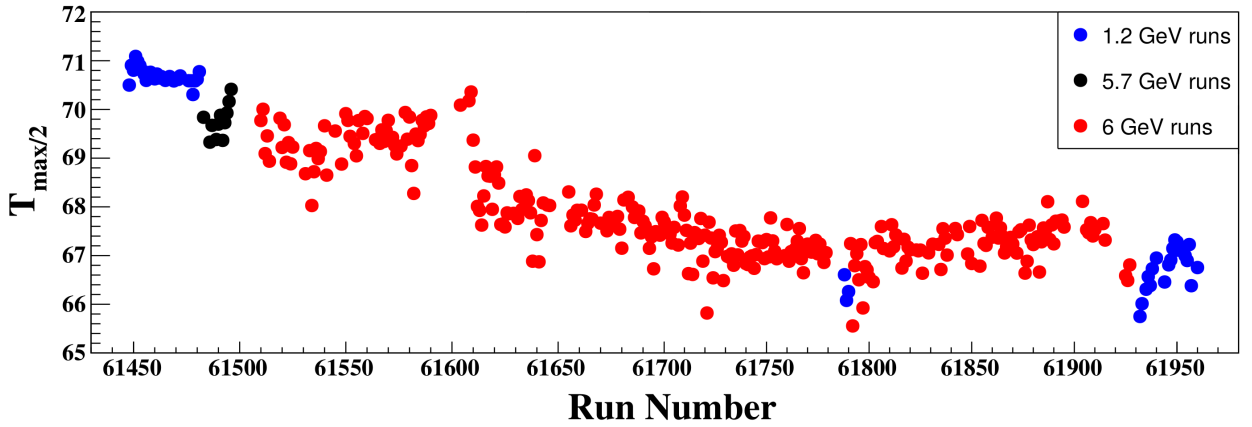


FIG. 9: $T_{max/2}$ versus the experimental run numbers.

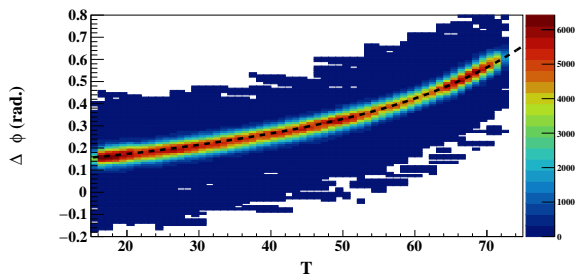


FIG. 10: $\Delta\phi$ versus T distribution in the second pass for tracks near 35 mm longitudinal position along the RTPC. The black line represents the final drift paths in this slice.

Interestingly, we found very similar drift paths for the two data sets and concluded that any changes in the system only significantly affected the drift speed.

C. Gain Calibration

The gain of each pad is defined as the ratio between the actual deposited energy and the registered ADC value. We tested two different methods to extract such gains, with varying degrees of success.

The first method is based on the measured average $\frac{dE}{dX}$ and the expected value based on the Bethe-Bloch formula. The total energy deposition for each ^4He track is calculated as the sum of all ADC hits attributed to the track. The path length of that energy deposition is calculated as the distance along the reconstructed trajectory between the first and last hits on the track and corrected to account for regions of bad channels along the track. The measured average energy loss is then the ratio of deposited energy and path length. The Bethe-Bloch formula is evaluated at the track's reconstructed momentum, and the ratio with the measured $\frac{dE}{dX}$ is taken as a gain scaling factor. This average gain is attributed

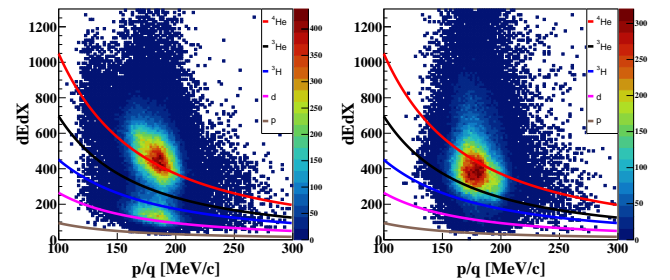


FIG. 11: $\frac{dE}{dX}$ vs. p/q distribution for the left half of the RTPC (left) and for the right half (right). Here, $\frac{dE}{dX}$ is calculated using the gains of the first method. The lines are theoretical expectations from Bethe-Bloch formula for ^4He , ^3He , ^3H and ^2H (d).

equally to each readout channel contributing to the track, and each channel's gain is averaged over many tracks. This gain calibration method is inherently iterative, and, while it does result in measured $\frac{dE}{dX}$ much closer to the expected Bethe-Bloch curve than prior to calibration, the results shown in figure 11 are not very satisfactory.

The second method is to compare the experimental ADCs to the energy deposited in GEANT4 by similar simulated tracks (using the same elastic events than for the drift paths calibration). This requires a very good GEANT4 simulation including drift paths, but also the spread of the charges along the path before reaching the pad, so that the simulated hits match the experimental ones. Moreover, the simulation has to match the data acquisition (DAQ) features that can lead to cutting out hits. After setting the simulation properly, we compared simulation to experiment on an event by event basis as shown in Figure 12. In this step, the gain for each pad is calculated as the ratio of the measured ADCs to the simulated deposited energy. Then, these gains are refined using correcting factors obtained from a sample of good tracks. For each track, we calculate the corrected

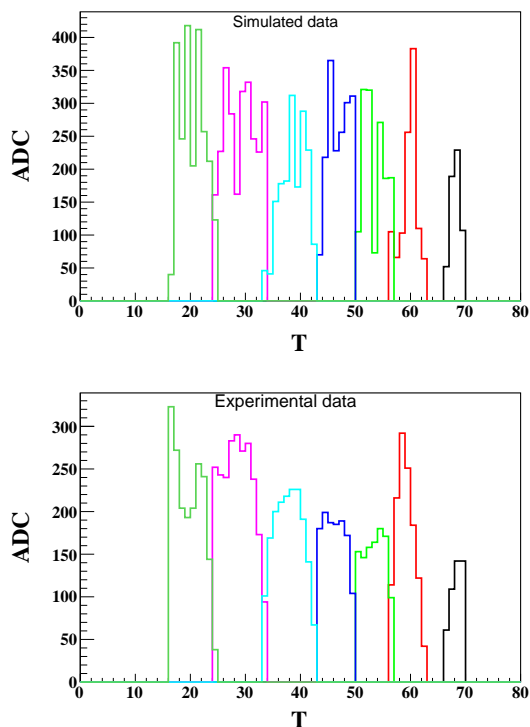


FIG. 12: Simulated (upper) and experimental (lower) ADC and T distributions of a track. The colors indicate the pads, same color in top and bottom indicate that they are the same pad.

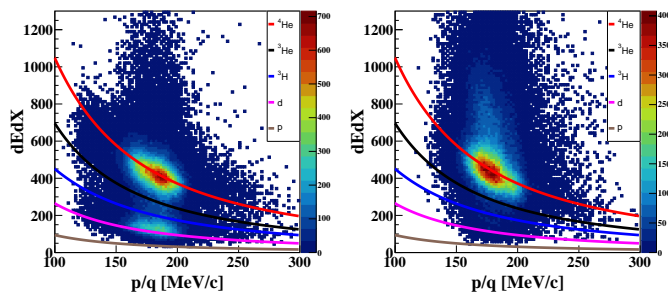


FIG. 13: $\frac{dE}{dX}$ vs. p/q distribution for the left half of the RTPC (left) and for the right half (right). Here, $\frac{dE}{dX}$ is calculated using the gains of the second method. The lines are theoretical expectations from Bethe-Bloch formula for ^4He , ^3He , ^3H and ^2H (d).

energy deposit on a pad and compare it to the average deposit recorded by the other pads. Results of this second method are shown in Figure 13, from these we concluded that the gains of the second method match best the theoretical lines.

D. Noise Rejection

Two independent noise signatures were identified in the raw data and removed in software prior to track reconstruction. Both are transient and isolated to a subset of the readout channels.

The first is an oscillatory noise located early in the readout time window, shown in the top panel of Figure 14 for a particularly noisy channel. Its amplitude is not dissimilar to those of real tracks, and about 18% of the readout channels exhibit large contributions from this noise characteristic. Due to its unique time-energy correlation for the given channels, the noise could be removed on an event by event and channel by channel basis without significant loss of good signals, and the result is illustrated in the bottom panel of Figure 14.

The second is a coherent noise affecting about 25% of the preamplifiers, where the signature is simultaneous hits in most of the 16 channels in a preamp group. An event-based technique to identify and remove it was developed based on counting simultaneous hits in preamp group, and, if sufficiently large, perform a dynamic pedestal subtraction based on the average ADC of the channels' neighbors within the preamp group.

The sources of these effects were not determined, but rejection techniques allowed to reconstruct 10% more good tracks, with no significant loss, and recover 70 channels that were previously ignored due to excessive noise levels.

V. TRACK RECONSTRUCTION

In order to reconstruct tracks we first select good hits. This means rejecting out-of-time hits and hits linked to the electronic noise. The second step is to reconstruct the spacial origin of the hits using the extracted drift speed and drift path parameters. For each registered hit, we calculate a position of emission from the recorded time and the position of the recording pad. The third step is to create chains of hits. The maximum distance between two close adjacent hits has to be less than 10.5 mm to chain them, this roughly correspond to neighbors and next to neighbors. Then, we fit the chains that have a minimum of 10 hits. We make the fit in two iterations, first, all the hits of the chain together with the beam line are fitted with a helix. For the second iteration, the hits that are 5 mm or farther from the first fit are excluded.

For energy deposition, the mean $\frac{dE}{dx}$ is calculated as

$$\left\langle \frac{dE}{dX} \right\rangle = \frac{\sum_i \frac{ADC_i}{G_i}}{L}, \quad (1)$$

where the sum runs over all the hits of the track, G_i is the gain of the associated pad, and L is the visible track length in the active drift volume.

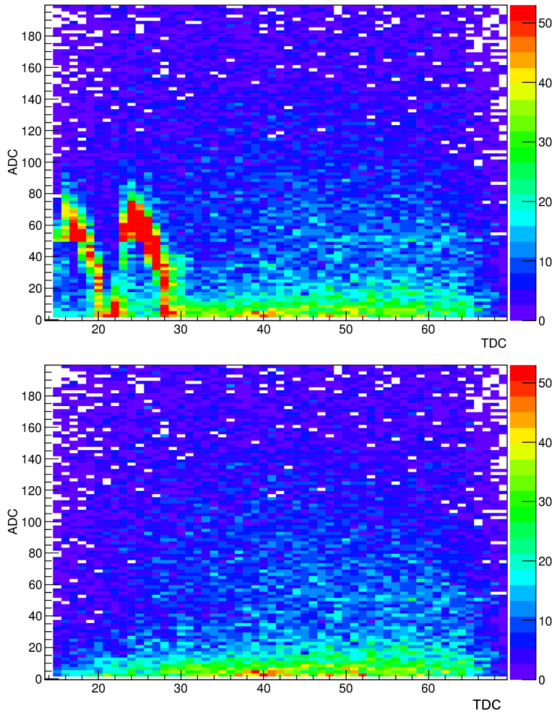


FIG. 14: The ADC vs. T spectrum for an example noisy channel before (top) and after (bottom) noise rejection algorithms. Only hits associated with tracks are included, and the selection of events and tracks is the same in both plots.

VI. PERFORMANCE STUDIES

The previous discussions have shown that the two modules of the RTPC have slightly different behavior and give also different particle yield. However, this should not necessarily be linked to a different performance of the RTPC. Indeed, there is a complicated convolution of CLAS and the RTPC acceptances that can significantly affect the yields and the kinematic of the detected particles. To clarify this question, we measured the efficiency

of the RTPC using the elastic scattering on ^4He , by comparing the the inclusive yield based on electron detection only to the exclusive elastic yield where we also detect the Helium recoil. We present in Figure 15 the results for the two modules of the detector. We observe that the left and the right modules have similar efficiencies except near the target windows, as shown in figure 15.

VII. CONCLUSION

We reported on the construction, operation and calibration of a small RTPC designed to measure helium-4 nuclei in high rate environment. The operation of the detector was successful and allowed to detect helium nuclei at a rate of 3.1 kHz in coincidence with the detection of high energy electrons and photons in the CLAS spectrometer.

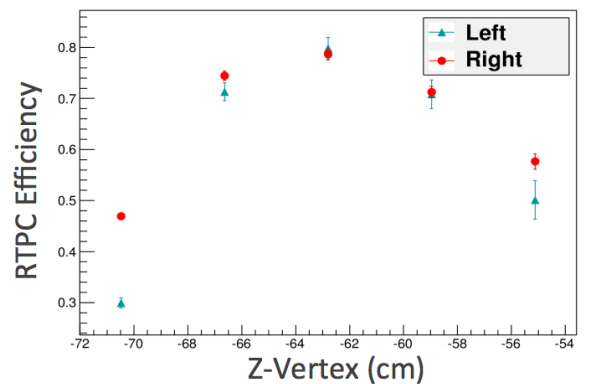


FIG. 15: The RTPC ^4He detection efficiency as a function of the longitudinal position along the detector.

We thank and acknowledge the support from Jefferson laboratory.

[1] B.A. Mecking et al., The CEBAF large acceptance spectrometer, Nucl. Inst. and Meth. A 503, 513 (2003).
 [2] M.D. Mestayer et al., The CLAS drift chamber System, Nucl. Inst. and Meth. A 449, 81 (2000).
 [3] G. Adams et al., The CLAS Cerenkov detector", Nucl. Inst. and Meth. A 465, 414 (2001).
 [4] E.S. Smith et al., The time-of-flight system for CLAS, Nucl. Inst. and Meth. A 432, 265 (1999).
 [5] M. Amarian et al., The CLAS forward electromagnetic calorimeter, Nucl. Inst. and Meth. A 460, 239 (2001).
 [6] Hyon-Suk Jo, Etude de la Diffusion Compton Profondément Virtuelle Sur le Nucléon avec le Détecteur CLAS de Jefferson Lab: Mesure des Sections Efficaces polarisées et non polarisées, IPNO-Thesis, 2007.
 [7] G Asryan et al., Meson spectroscopy in the Coherent

Production on ^4He with CLAS, Jlab proposal to PAC31 (2007).
 [8] K. Hafidi et al., Deeply virtual Compton scattering off ^4He , Jlab proposal to PAC33 (2008).
 [9] F. Sauli, The Gas Electron Multiplier (GEM): Operating Principles and Applications, Nucl. Instr. and Meth, A805(2016)2
 [10] J. Beringer et al. (Particle Data Group), Particle detectors at accelerators, Phys. Rev. D 86, 010001, pages: 339-368, 2012.
 [11] S. Biagi, Monte Carlo simulation of electron drift and diffusion in counting gases under the influence of electric and magnetic fields, Nucl. Inst. and Meth. in Phy. Res. A, vol. 421, pp. 234-240, 1999.
 [12] Howard C. Fenker et al., BoNuS: Development and Use

- of a Radial TPC using Cylindrical GEMs, Nucl. Instrum. Meth. A592, 273-286 (2008)
- [13] L. Musa et al., The ALICE TPC front end electronics, 2003 IEEE Nuclear Science Symposium, 2003, pp. 3647-3651 Vol.5
- [14] H. K. Soltveit *et al.*, “The Preamplifier shaper for the ALICE TPC-Detector,” Nucl. Instrum. Meth. A **676** (2012) 106
- [15] , R. E. Bosch, *et al.*, “The ALTRO chip: a 16-channel A/D converter and digital processor for gas detectors”, IEEE Transactions on Nuclear Science, vol. 50, no. 6, pp. 2460-2469, Dec. 2003.
- [16] <http://geant4.cern.ch>
- [17] It was noted during the experiment that leaks appeared and the gas flow had to be increased in few occasions to compensate for this.